Absorption, luminescence and scattering of single nano-objects

Yorulmaz, M.

Appendices

APPENDIX A

The dissipated power for some common chromophores

Here we estimate the dissipated power in photothermal experiments with single molecules. A single molecule modelled as a two-level system can release heat via two pathways: (i) through non-radiative transitions (internal conversion) from the excited state, and (ii) through vibronic relaxation prior to or after a radiative (fluorescence) transition.

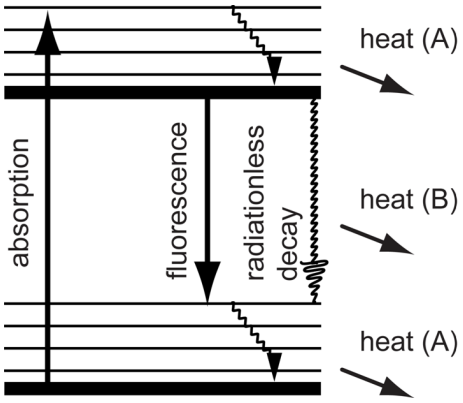

Figure A.1: Simple level scheme representing a single molecule. Absorbed energy either leads to fluorescence emission or/and can be transformed into heat. The dissipation of energy into heat goes through (A) vibronic relaxation, and (B) radiationless decay. For an organic molecule at saturation, the calculated dissipated power p_{diss} is given in Table A.1.

The power (p_{diss}) dissipated as heat into the surrounding medium by a single molecule depends on the absorbed power ($P_{abs} = \sigma_{sm} \cdot P_{heat}/A$) provided by the heating beam (or excitation) focused into the spot of area A, the fluorescence quantum yield ($\eta_F = k_r/(k_r + k_{nr})$), defined by the radiative lifetime ($\tau_r = 1/k_r$) and the non-radiative lifetime ($\tau_{nr} = 1/k_{nr}$) of the excited state of the molecule. The fluorescence lifetime ($\tau_F = 1/(k_r + k_{nr})$) is defined by the contribution of the radiative and non-radiative transitions. The dissipated power can be written as follows:

$$p_{diss} = P_{nr} + P_{fluor} = P_{abs} \cdot \eta_{diss} = P_{abs} \left[(1 - \eta_F) + \eta_F \frac{h\nu_{exc} - h\nu_{fluor}}{h\nu_{exc}} \right] \quad \text{(A.1)}$$

where ν_{exc} and ν_{fluor} are frequencies of excitation and fluorescence, $P_{heat} = P_{exc}$ is the power of the heating laser (fluorescence excitation), η_{diss} is the dissipation yield.

In the approximation of a two-level system the heating laser power required for absorption saturation P_{heat}^{sat} is given by the following equation:

$$P_{heat}^{sat} = h\nu_{heat}\frac{1}{\tau_F}\frac{A}{\sigma_{sm}} \tag{A.2}$$

Table A.1: Calculations of the dissipated power for several commercial organic molecules. τ_F is the fluorescence lifetime. η_{fluor} is the fluorescence quantum yield and η_{diss} is the dissipation yield. The absorption cross-sections for molecules (σ_{sm}) are calculated based on the manufacturer's data for extinction coefficients. Heating laser power at absorption saturation (P_{heat}^{sat}) is calculated according to Eq.A.2, assuming the 514 nm excitation light focused into a diffraction-limited spot. The dissipated power (p_{diss}) is calculated for two cases: (i) in the approximation of a saturated optical transition, and (ii) if possible, with a heating power of $P_{heat} = 5.1$mW.

						p_{diss} (nW)	
Dye	τ_F (ns)	η_{fluor}	η_{diss}	σ_{sm} (nm^2)	P_{heat}^{sat} (mW)	at saturation	with $P_{heat} =$ 5.1mW
Rh6G	4.08	0.95	0.08	0.043	0.5	0.015	0.015
Cy3	0.3	0.04	0.96	0.057	4.4	2.5	2.5
Cy5	1	0.4	0.61	0.096	0.8	0.5	0.5
BHQ1 *	0.05	-	1	0.013	117	15	0.34
ErB †	0.61	0.12	0.88	0.04	3.1	1.1	1.1
CV ‡	0.1	0.019	0.98	0.037	20	7.6	0.94

The lifetime of BHQ1 is unknown. We estimated it to 50 ps from those of similar azo dyes. The fluorescence quantum yield is also uncertain and was deduced from the lifetime. As we can see from the Table A.1, the chromophore we selected for our experiments, BHQ1, has the highest dissipated power in the saturation limit (15 nW), and Rh6G - the lowest one (0.015 nW). The dissipated powers for the experimental heating power of 5.1 mW focused into a diffraction-limited spot are about 1 nW. These small dissipated powers can be detected in photothermal experiments with an acceptable SNR, provided suitable integration time and probe power are chosen. We note that the

*black-hole-quencher[126,127,130,257]

†erythrosine[36,258]

‡crystal violet[259,260]

high heating powers required in single-molecule photothermal microscopy also require a good photostability of the absorbers. This is difficult to achieve with most of the weakly fluorescent dyes (Cy3, CV, etc.).

APPENDIX B

Organic dye nanoparticles

AFM studies of fvin nanoparticles

The results obtained from height measurements of fvin NPs is shown.

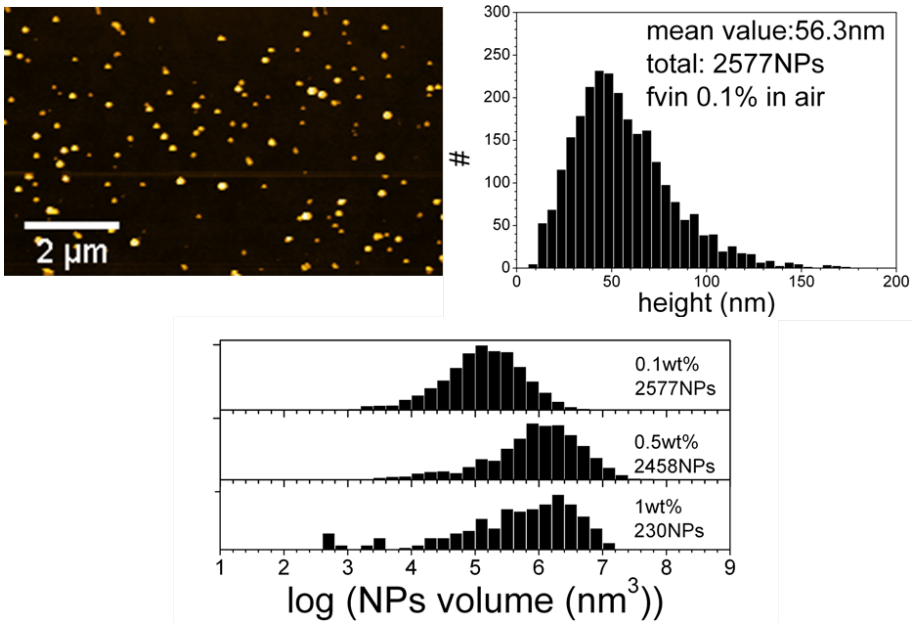

Figure B.1: A typical AFM image (top, left) and a histogram of heights (top, right) of fvin NPs prepared from a 0.1 wt% stock solution, and deposited on APTES glass by spin-coating. Measurements are done in tapping mode in air. The average diameter of fvin NPs is 56 nm, as estimated from the average height in AFM images. (Bottom) Histograms of the volumes of NPs estimated from the heights measured by AFM for various fvin concentrations.

These histograms reveal large variation of NPs volumes (more than 10 times). This observation corresponds well with the distribution of photothermal signals (Photothermal signal is proportional to the volume of NPs) obtained in the photothermal microscopy experiments. The average volume of 0.1 wt% fvin NPs is 4×10^5 nm^3.

Bulk absorption and luminescence properties of fvin dye and nanoparticles

We give information about the chemical structure of the organic dye (fvin) used for fvin nanoparticles (fvin NPs) preparation together with bulk absorption and luminescence spectra of nanoparticles.

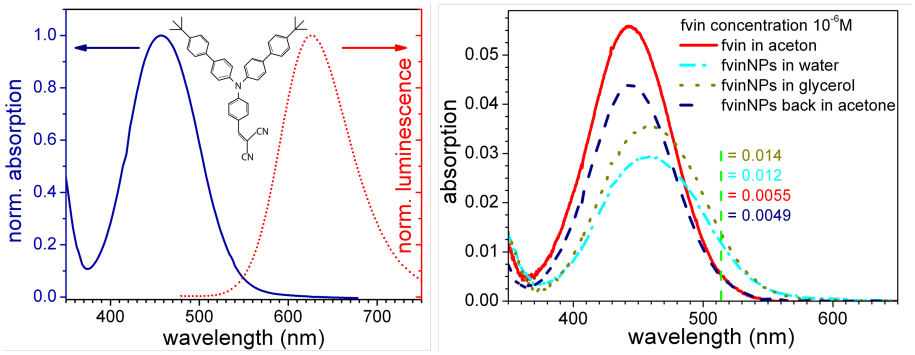

Figure B.2: Bulk spectroscopy experiment results. (left) Normalized absorption (solid) and luminescence (dot) spectra of 0.1 wt% fvin nanoparticles in water. Absorption and emission maximums are at about 450 nm and 620 nm, respectively. Since luminescence is largely red-shifted, fvin NPs do not suffer from re-absorption. Inset shows the chemical structure of the organic dye (fvin) used for nanoparticles preparation (right) Absorption spectra of fvin dye in acetone (solid), 0.1 wt% fvin NPs in water (dash-dot), 0.1 wt% fvin NPs in glycerol (dash), and 0.1 wt% fvin NPs placed back from the water solution into acetone (dash) measured at the constant concentration of fvin dye of 1.67×10^{-6} M. Absorption maximum in acetone is at 443 nm and the molar extinction coefficient is $\varepsilon(\lambda = 443\,\text{nm}) = 33400\,\text{Lmol}^{-1}\text{cm}^{-1}$. Absorption maximum in glycerol is at 458 nm and the molar extinction coefficient is $\varepsilon(\lambda = 458\,\text{nm}) = 21300\,\text{Lmol}^{-1}\text{cm}^{-1}$.

Photothermal and fluorescence microscopy of fvin NPs at low and high heating power regimes

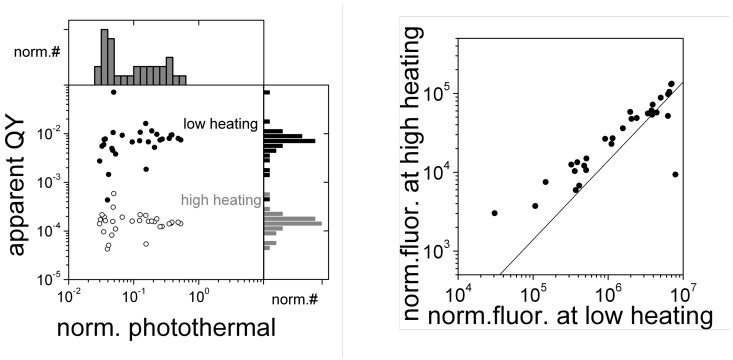

Figure B.3: (left) A scatter plot presenting apparent fluorescence quantum yield for the same data as in Fig. 3.2 C (right) A correlation of normalized fluorescence from the same fvin NPs consequently measured at two excitation regimes. A solid line presents a linear correlation with the slope of 1 on the log-log scale.

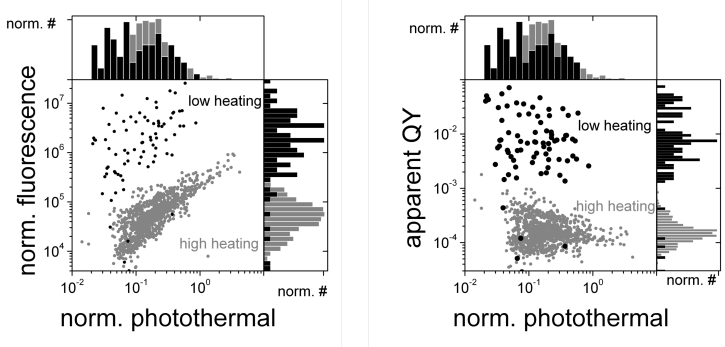

Figure B.4: (Left)A correlation of normalized fluorescence and normalized photothermal signals in two regimes of heating power: low heating power less than 2 μW (black, 83 NPs), and high heating with $85 - 128$ μW (light grey, 1268 NPs). Top and right panels show histograms for photothermal and fluorescence signals, correspondingly. (right) Apparent quantum yield as a function of normalized photothermal signal. The probe power used in the experiments is 23-56 mW. The acquisition time for fluorescence signal per pixel was 10 ms, and 3 ms lock-in integration time for the photothermal signal.

Annihilation and apparent quantum yield

We show the effect of annihilation (singlet-singlet or single-triplet) — quenching of an excited state by other excited states in the surrounding — on the luminescence count-rate of fvin nanoparticles and accordingly on the quantum yield. We observe a decrease in the quantum yield at high excitation regime.

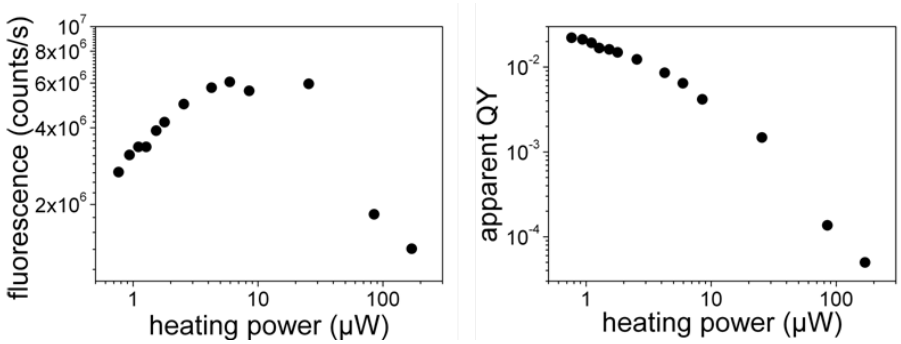

Figure B.5: (left) Fluorescence signal from individual fvin NP (0.5 wt%) as a function of the heating power. Two regions can be indicated: (i) low heating power regime with the power less than 5 μW, where fluorescence signal grows with the heating power; (ii) high heating power regime, where the apparent fluorescence signal decreases with the heating power due to combined effects of fluorescence quenching and bleaching. (Right) The calculated apparent fluorescence quantum yield as a function of the heating power. The value of the absorption cross-section for the fvin NPs is assumed to be constant in these calculations.

Calculation of number of dye molecules in a nanoparticle

We calculate the number of fvin dye molecules in fvin NPs in three independent ways.

(i) based on the photothermal signal from NPs:

The extinction coefficient of dye compound in glycerol (ε_{dye}) is 8400 $Lmol^{-1}cm^{-1}$ at 514 nm. The average isotropic absorption cross-section of a single dye (σ_{dye}) is calculated as follows:

$$\sigma_{dye}(cm^2) = 1000 \cdot \ln(10) \frac{\varepsilon_{dye}}{N_A} \sim 3.2 \times 10^{-3} nm^2$$

where N_A is the Avogadro constant.

The average absorption cross-section of individual fvin nanoparticles in glycerol is found to be $\sigma_{fvinNP} \approx 180\ nm^2$. (The absorption cross-section of each individual fvin NP was estimated by comparing photothermal signal of each fvin NP with the average photothermal signal from individual 20 nm diameter gold NPs under same illumination conditions).

We further assume that free fvin dye molecules and fvin dye molecules in nanoparticle have similar, but anisotropic absorbance. Thus, the number of dye molecules per average fvin NP is calculated as follows:

$$\frac{\sigma_{fvinNP}}{\sigma_{dye}} = \frac{180}{3.2 \times 10^{-3}} \approx 6 \times 10^4$$

(ii) based on the photoluminescence signal from NPs:

The photoluminescence quantum yield (QY) can be estimated as follows:

$$QY = \frac{N_{em}}{N_{abs} \times Det.Eff.}$$

where N_{em} is the number of the emitted photons, N_{abs} is the number of the absorbed photons, and $Det.Eff.$ is the detection efficiency (5%). The average number of photons emitted by a fvin NP is $N_{em} \sim 600$ kcounts/s for the excitation intensity of 1.7 kW/cm^2. Taking into the account the average QY of 10^{-2} for fvin NPs in the low heating power regime, the average number of absorbed photons by fvin NPs is $(N_{abs})_{fvinNPs} \sim 1.2 \times 10^9$.

The number of absorbed photons by a dye molecule is estimated as follows:

$$(N_{abs})_{dye} = \frac{\sigma_{dye} I}{h\upsilon} \approx 1.4 \times 10^5$$

where σ_{dye}, I and $h\upsilon$ are absorption cross-section of dye compound, laser intensity and energy of a photon, respectively.

Thus, the number of molecules per fvin NP is: $\frac{(N_{abs})_{fvinNPs}}{(N_{abs})_{dye}} \approx 10^4$

(iii) based on the measurements of diameters of NPs by means of AFM:

The average diameter of fvin NPs is 3.2×10^5 nm^3 (See Fig. B.1). The molecular Van der Waals volume of fvin is 0.85 nm^3. Then, the average number of molecules per fvin NP is about 4×10^5.

Table B.1: Parameters for calculations of the average number of molecules in fvin NPs.

	$\sigma(nm^2)$*	N_{abs} $(photons/s)$ †	Volume (nm^3)
fvin NP	180	1.2×10^9	4×10^5
fvin dye, isotropic	3.2×10^{-3}	1.4×10^5	0.85
$\frac{\#\ of\ molecules}{fvinNP}$	6×10^4	10^4	5×10^5

*at 514 nm

†at excitation intensity of 1.7 kW/cm^2

APPENDIX C

Single gold nanospheres

Correction factor for the luminescence efficiency

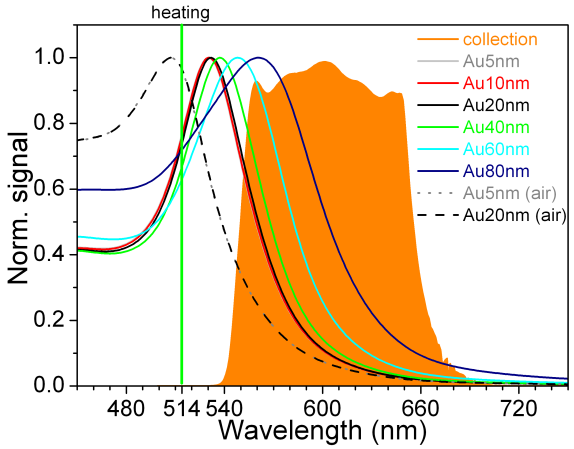

Figure C.1: Normalized absorption spectra for gold NPs of various sizes immersed in glycerol or in air (lines) and the normalized transmission spectrum of optics in fluorescence detection path (shaded area). The variable overlap between detection and emission spectra leads to adjustment factors for the quantum yield. The calculated factors for different sizes of gold nanospheres are given below in Table C.1. We assume the emission spectrum to follow the absorption on the long-wave side.

Table C.1: Correction factors for the luminescence efficiency. In order to calculate the correction factor, we compare the area under the absorption spectrum and the area of overlapping region of absorption and transmission spectrum for each nanosphere over the wavelength range of 480 nm to 800 nm.

Diameter (nm)	Norm. total abs. (a.u.)	Norm. trans. of abs. spectrum (a.u.)	QY mult. factor *
5 (air)	67	11	6.1
10	71	18	3.9
20	71	18	3.9
40	71	19	3.7
60	76	24	3.2
80	89	37	2.4
20 (air)	67	11	6.1

*The correction factor is subject of a possible error. Exact values have to be estimated based on measurements of luminescence spectra of individual NPs.

APPENDIX D

Single gold nanorods

Extinction spectrum of nanorods and nanospheres

The normalized extinction spectra of the nanorods shown in Fig. D.1 exhibit two peaks. The peak at around 515 nm-520 nm corresponds to the transverse plasmon resonance and a contribution from spherical particles present in the nanorod suspension. The red-shifted peak corresponds to the longitudinal plasmon resonance. The normalized extinction spectrum of gold nanospheres with ensemble averaged diameter of 18.5 nm has a single peak at 525 nm.

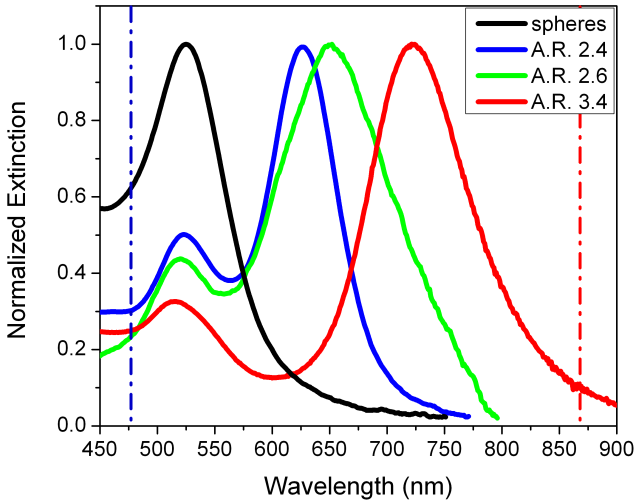

Figure D.1: Extinction spectra of nanorod and nanosphere suspensions in water measured using UV-VIS spectrophotometer. Blue, green and red solid curves correspond to suspension of nanorods with ensemble average aspect ratios (A.R.) of 2.4, 2.6 and 3.4, respectively. Black curve corresponds to the suspension of 18.5 nm diameter gold nanospheres. Dashed-dotted lines show the excitation (476 nm) and probe laser wavelengths (864 nm) used in the experiment.

Setup for combined fluorescence and scattering microscopy

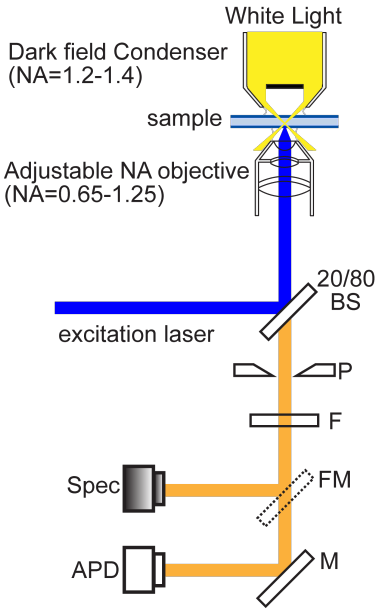

Figure D.2: Schematic of the experimental setup for correlation of scattering and luminescence signals of nanorods. M - mirror, FM - flip mirror,F - filter, P - pinhole, BS - beam splitter, Spec - spectrometer, APD - avalanche photodetector.

For luminescence imaging, the luminescence signal of nanoparticles, which was obtained by excitation at 476 nm, was spatially filtered by a 50 μm pinhole and spectrally selected by a set of longpass filters (LP02-514RU-25 and LP02-514RS-25, Semrock). The raster-scan luminescence images were recorded by focusing the luminescence signal on a single-photon-counting avalanche photodetector (SPCM-AQR-16, Perkin Elmer). The luminescence signal which was filtered out from excitation laser was also directed towards a spectrometer (SpectraPro500i) with the help of a flip mirror for spectra measurements. It was collimated and then focused on a 200 μm slit and dispersed by a 150 g/mm grating and finally detected by a liquid nitrogen cooled CCD (PI Acton SPEC10:400).

Scattering spectra were measured in a dark-field geometry using a 150 W halogen light source (Thorlabs). The experiment was performed using a microscope objective with a variable numerical aperture (NA) (Olympus, 60X oil immersion, 0.65-1.25 NA) and a dark-field condenser (Olympus, 1.2-1.4 NA). To facilitate the correlation between scattering and luminescence spectra of the same particle, we used the same focusing objective set at 1.25 NA to record the luminescence spectra or set to 0.65 NA for dark-field spectroscopy.

Temperature rise on the surface of nanorods

The maximum temperature increase on the surface of a gold nanorod is calculated by $\Delta T_{surf} = \sigma_{NR} I_{exc} / 4\pi\kappa R$ where I_{exc} is the excitation laser intensity, σ_{NR} is the absorption cross-section of the nanorod at the wavelength of the excitation laser, κ is the thermal conductivity of the medium (glycerol), and R is the equivalent radius of the particle which has absorption cross section of σ_{NR}. Temperature rises on the surface of nanorods of Fig. 5.3 (in Section 5.3) are shown in Fig.D.3. We obtained the laser intensity from the full-width-at-half-maximum σ of the photothermal and luminescence spots along the x- and y-axis by a Gaussian fit. This yielded values for σ_x and σ_y of 260 nm and 340 nm for photothermal spots and 320 nm and 360 nm for the luminescence spots.

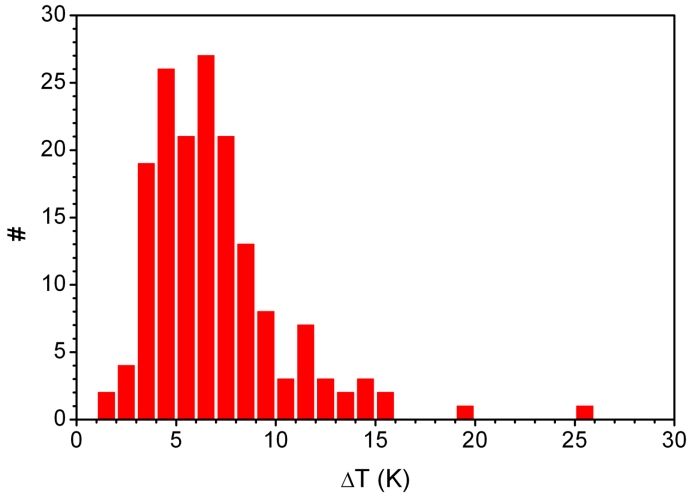

Figure D.3: The histogram of the laser-induced ΔT_{surf} on nanoparticles shown in Fig. 5.3 (in Section 5.3). The average surface temperature is $\Delta T_{surf,av} = 7 \pm 3$ K.

Signature of clustered particles

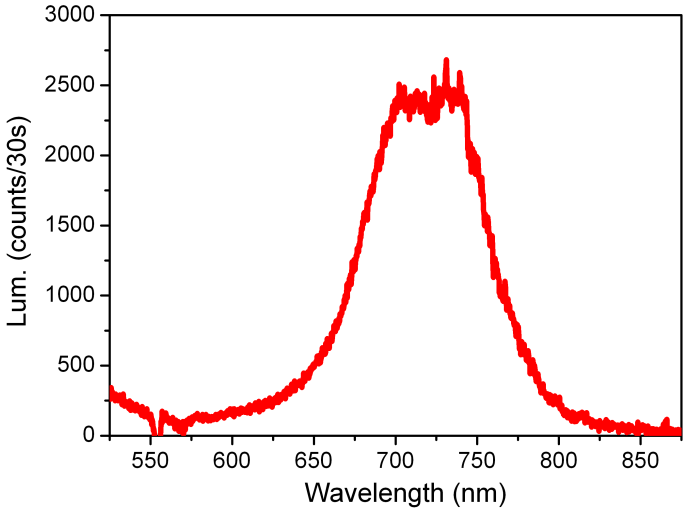

Figure D.4: An example of luminescence spectrum which does not belong to a single particle.

The shape and width of luminescence spectra provides us information to distinguish single Au nanorod from aggregates. The luminescence spectrum shows a non-Lorentzian shape or double peak when it belongs to aggregated nanorods.

An example of control experiments to ensure there is no reshaping of particles

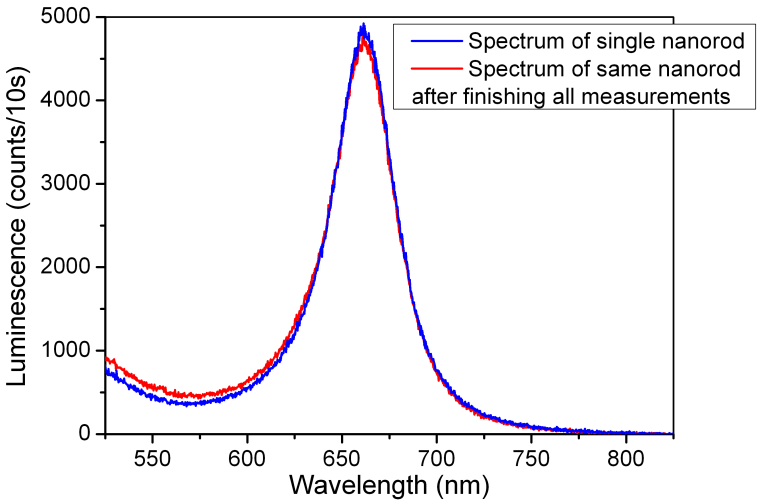

Figure D.5: The luminescence spectrum of a single gold nanorod before and after performing all optical measurements. This has been checked for each sample to ensure there was no significant reshaping of the particles for the measurements of the QY.

Excitation power dependence of photothermal and luminescence signal

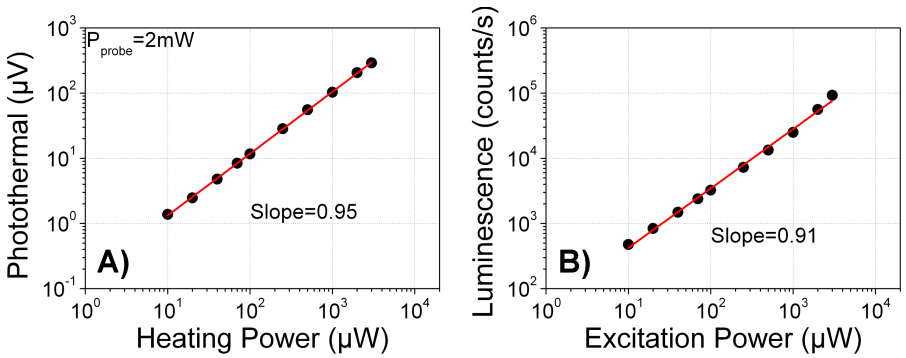

Figure D.6: Power dependence of (A) photothermal and (B) luminescence signal. The linear relationship between the excitation power and the luminescence intensity confirms that the observed luminescence is one-photon luminescence.

Transmittance of optics and the detection efficiency

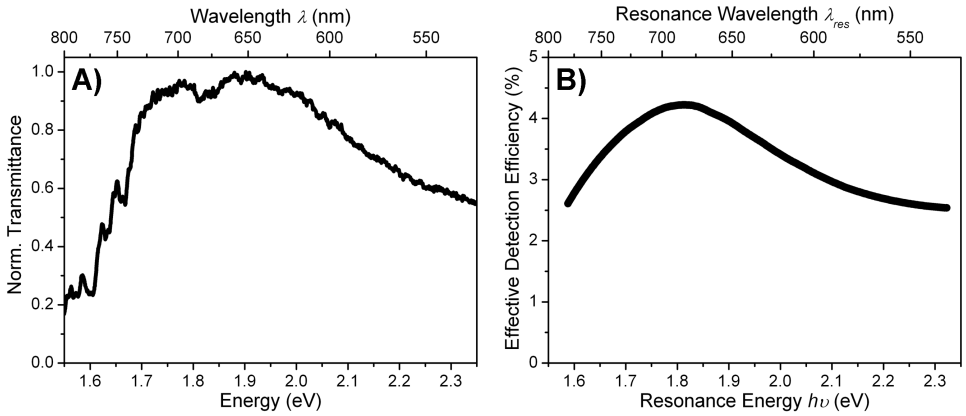

Figure D.7: (A) Normalized transmittance of optics with spectrometer efficiency, $T(\lambda) \times F(\lambda)$, as a function of photon energy (wavelength - top axis). (B) Calculated effective detection efficiency of setup, $\Pi_{setup}(\lambda_{res})$, as a function of nanorod plasmon resonance energy (resonance wavelength - top axis).

In order to obtain the luminescence spectrum of a nanorod, $I(\lambda)$, the measured spectrum, $S(\lambda)$, was corrected for the transmission of optics, $T(\lambda)$, including the spectrometer efficiency, $F(\lambda)$, as follows:

$$I(\lambda) = \frac{S(\lambda) - B(\lambda)}{T(\lambda) \times F(\lambda)}$$

where $S(\lambda)$ is the measured spectrum of a nanorod, $B(\lambda)$ is the background signal and $T(\lambda) \times F(\lambda)$ is the normalized transmittance of optics including the efficiency of the spectrometer.

For the calculation of the quantum yield, we used the detection efficiency of setup, $\Pi_{setup}(\lambda_{res})$ which was calculated as follows:

$$\Pi_{setup}(\lambda_{res}) = \frac{5\%}{C(\lambda_{res})}; C(\lambda_{res}) = \frac{\int I(\lambda) d\lambda}{\int I(\lambda) T(\lambda) A(\lambda) d\lambda}$$

where $C(\lambda_{res})$ is the calculated correction factor for a nanorod with luminescence spectrum $I(\lambda)$ and plasmon resonance λ_{res}. $T(\lambda)$ is the transmission of optics and $A(\lambda)$ is the efficiency of APD.

Volume effect on QY

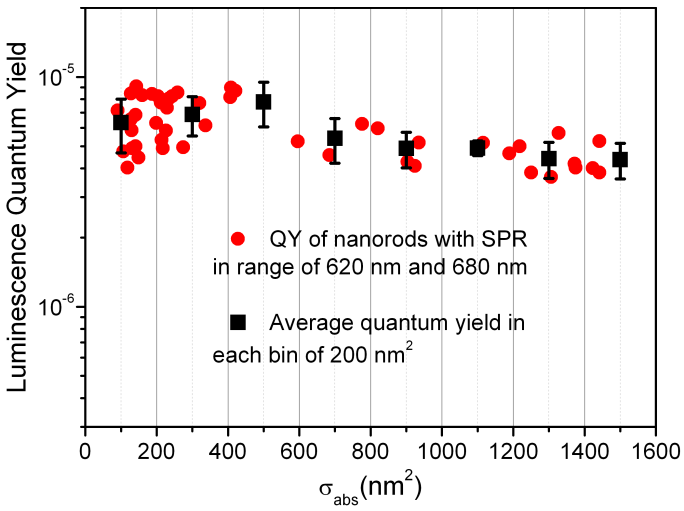

Figure D.8: Luminescence QY as a function of absorption cross-section of nanorods with similar surface plasmon resonance in range of 620 nm and 680 nm. Red-filled-circles are data of individual nanorods. Black-filled-squares are the averages of QY in bins of 200 nm^2 where error bars show the standard deviation of the mean.

Medium effect on the luminescence spectrum of a single gold nanorod

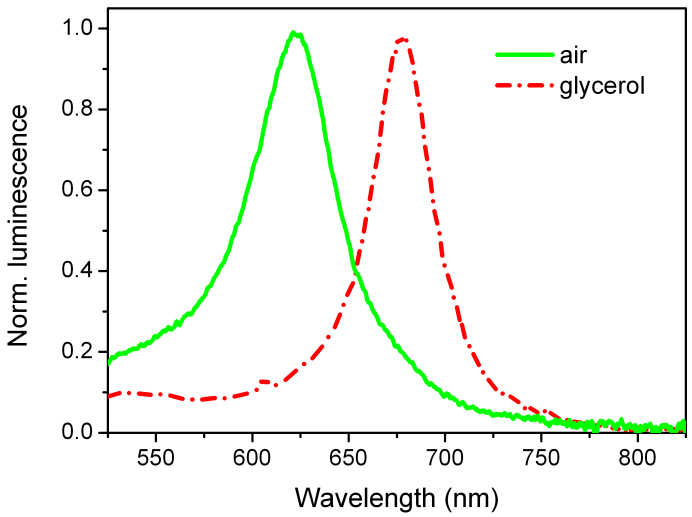

Figure D.9: Photoluminescence spectra of a single gold nanorod in air (green-solid line) and in glycerol (red dashed-dotted line). The plasmon wavelengths are 625 nm and 680 nm in air and in glycerol, respectively. The excitation wavelength is 514 nm.

We observed a plasmon peak shift of ∼55 nm when the medium was changed from air to glycerol. The observed shift is due to the change of the effective refractive index from 1.25 (glass-air interface) to 1.5 (glass-glycerol interface) and is close to the expected difference of ∼50 nm.

Volume dependence of the ”green” emission component

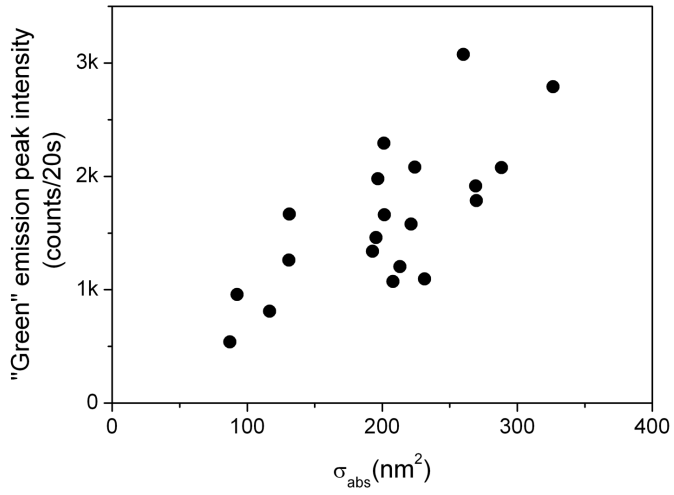

Figure D.10: Intensity of the ”green” component contribution as a function of the calculated absorption cross section of the nanorods. The ”green” emission peak intensity was obtained from the mean of luminescence intensities over 525 nm and 530 nm for each particle. The absorption cross sections of nanorods were obtained as described in the main text. The ”green” component we observe is peaked at 500 nm, and its intensity scales as the volume of the particle (as deduced from photothermal measurements).